Research Article **Open Access**

Zheyuan Zhang, Yonghui Xie*, Di Zhang, and Gongnan Xie

Flow Characteristic and Heat Transfer for Non-Newtonian Nanofluid in Rectangular Microchannels with Teardrop Dimples/Protrusions

DOI 10.1515/phys-2017-0021
Received July 29, 2016; accepted October 31, 2016

Abstract: Porous cavity technology is one of the effective ways to improve local flow structures and thus the overall heat transfer of heat exchanging devices. In the present investigation, the flow characteristics and heat transfer in a microchannel heat sink with teardrop dimples/protrusions are studied with a numerical method. The working substances are Al_2O_3-water nanofluids, which are defined by power-law shear-thinning model. The relative depth and positive eccentricity of dimples/protrusions arranged in the microchannels are 0.2 and 0.3 respectively. The inlet velocity varies in the range of 1.41 $m \cdot s^{-1}$ to 8.69 $m \cdot s^{-1}$ and the volume fraction ranges from 0.5% to 3.5%. The effects of the flow and heat transfer characteristics are investigated by analyzing the limiting streamlines structures and temperature distributions. The overall thermal performance is evaluated by parameters of Fanning friction factor, Nusselt number and thermal performance. It is shown that the combination of teardrop dimple/protrusion structure and Al_2O_3-water nanofluids could effectively strengthen heat transfer with low pressure loss. Moreover, in order to obtain the best overall thermal performance, working substances with volume faction of 3.5% is preferred for the proposed microchannel structure.

Keywords: Microchannel heat sink; Nanofluids; Flow characteristics; Heat transfer; Teardrop dimple/protrusion

PACS: 44.30.+v

1 Introduction

In some industries, a normal cavity can be replaced by a novel porous cavity to achieve better overall thermal performance. With the development of high efficiency compact heat exchanger devices, traditional heat transfer enhancement techniques no longer adapt to the requirement of larger heat flux. For this reason, the heat transfer method by means of working fluids innovation is proposed recently [1].

With the advantage of high thermal conductivity and considerable improvement of forced convective heat transfer, nanofluids are playing a significant role in heat exchanging systems, which has led to several recent research into the flow of nanofluids in porous media. By using a mathematical model, Sheremet [2] investigated the heat transfer characteristics of the steady natural convection in a kind of enclosed porous space filled with nanofluids. It was found that the local Nusselt number at the interface of solid wall and porous medium is directly related to five key parameters. The Finite Difference Lattice Boltzmann Method was first used to conduct the research of heat transfer and entropy behavior by Kefayati et al. [3]. This work simulated the natural convection of non-Newtonian laminar flow in a square-shaped porous cavity. Besides, the heat transfer of nanofluids, which is in a square cavity filled with porous media, is studied by Bourantas et al. [4] using a kind of meshless technique. He also investigated the effect of the porous medium on the nanofluid cooling efficiency. Sheremet and Pop [5] used numerical simulation to study the transient natural con-

Zheyuan Zhang: Shaanxi Provincial Engineering Laboratory of Turbomachinery and Power Equipments, Xi'an Jiaotong University, Xi'an, Shaanxi Province 710049, China
***Corresponding Author: Yonghui Xie:** Shaanxi Provincial Engineering Laboratory of Turbomachinery and Power Equipments, Xi'an Jiaotong University, Xi'an, Shaanxi Province 710049, China, E-mail: yhxie@mail.xjtu.edu.cn
Di Zhang: Key Laboratory of Thermal Fluid Science and Engineering of Ministry of Education, Xi'an Jiaotong University, Xi'an, Shaanxi Province 710049, China
Gongnan Xie: Department of Mechanical and Power Engineering, School of Marine Science and Technology, Northwestern Polytechnical University, P. O. Box 24, Xi'an, Shaanxi Province 710072, China

vection of a nanofluid in a wavy-shaped cavity with porous media. Rashidi et al. [6] conducted a theoretical study on the thermo convective boundary layer for a kind of viscoelastic power-law non-Newtonian fluid flowing over a porous wedge.

Meanwhile, the heat transfer and flow characteristics of non-Newtonian nanofluids has attracted many researchers in other fields. Singh and Harikrishna [7] combined three concentrations of alumina nanofluids and two microchannels to investigate the heat transfer behavior. The laminar convective thermal characteristics of an alumina-water solution, as a typical nanofluid, was researched by Kalteh et al. [8] numerically and experimentally. In his research, a kind of rectangular microchannel was adopted. Wen and Ding [9] conducted an experiment to investigate the heat exchange of Al_2O_3 aqueous solutions in a copper tube. They found that the enhancement degree of heat transfer rate increased with the growth of the Reynolds number and particle concentration of solutions. Santra et al. [10] first used power-law model to describe the viscosity of Al_2O_3 aqueous solutions. The natural convective behavior of a non-Newtonian nanofluid, which flows between two flat plates, was analyzed by Hatami and Ganji [11] with analytical and numerical methods. Xie et al. [12] studied the flow and heat transfer characteristics of a CMC aqueous solution, as a kind of typical shear thinning fluid, in dimpled/protrusioned microchannels numerically.

Previous work has shown that dimple/protrusion structures could effectively strengthen the overall thermal performance, and the microchannels have advantages in heat transfer process because of their large heat exchange coefficient and high surface to volume ratio. Chyu et al. [13, 14] proposed a novel passive controlling structure, a teardrop dimple to enhance the heat transfer. The results indicate that the flow in teardrop dimpled passages showed better thermal performance than that in hemispherical dimple at cases investigated. After that, Qu et al. [15] researched the flow structure and thermal performance of teardrop dimples and protrusions with various eccentricities, compared with hemispherical dimples/protrusions using a numerical method. The results show that, among the cases discussed, thermal performance (*TP*) reached the maximum value in the cases of teardrop dimples and protrusions with eccentricities e/D_h =0.4. The flow structures and heat transfer in microchannel were studied with experimental and numerical methods by Lee [16].

According to the literature review given above, teardrop dimples/protrusions and non-Newtonian nanofluids both have the potential to obtain better thermal performance. In the present research, a numerical investigation is carried out to analyze the flow characteristics and heat transfer of Al_2O_3-water (AW) nanofluids in teardrop dimpled and protrusioned passages for the purpose of observing the thermal performance of non-Newtonian fluids flowing in microchannels.

2 Physical properties of non-Newtonian fluid

The thermal physical properties of nanoparticles (Al_2O_3) and base fluid (H_2O) as are given in Table 1.

Table 1: Thermal physical properties of Al_2O_3 and H_2O.

Property	Al_2O_3	H_2O
Specific Heat C_p(J·kg^{-1}·K^{-1})	765	4179
Density ρ(kg·m^{-3})	3870	997.1
Thermal Conductivity λ (W·m^{-1}·K^{-1})	40	0.6

The specific heat and density of nanofluids are calculated by the equations as follows [20]:

$$\rho_{nf} = (1 - \phi)\rho_f + \phi\rho_p \tag{1}$$

$$C_{pnf} = (1 - \phi)C_{pf} + \phi C_{pp} \tag{2}$$

where φ, ρ and C_p represent volume fraction, density and specific heat capacity, respectively. The subscripts 'p', 'f' and 'nf' indicate nanoparticles, base fluids and nanofluids respectively. Equation (3) has been adopted to determine the effective thermal conductivity of aqueous solutions with spherical nanoparticles [20].

$$\lambda = \lambda_f \left[\frac{(\lambda_p + 2\lambda_f) - 2\phi(\lambda_f - \lambda_p)}{(\lambda_p + 2\lambda_f) + \phi(\lambda_f - \lambda_p)} \right] \tag{3}$$

where λ_f and λ_p represent thermal conductivity of the base fluid and nanoparticles, respectively. The non-Newtonian power-law model is described by

$$\tau = k\gamma^n \tag{4}$$

where τ, γ, n and k are the shear stress, shear rate, behavior index and consistency index of power-law fluids, respectively.

Based on the data and equations stated above, the corresponding thermal physical properties of Al_2O_3 aqueous solution with different volume fraction are shown in Table 2. Besides, the shear-thinning model has been used to

define the viscosity of this kind of nanofluid [10] and details are shown in Table 2.

3 Physical model and numerical method

3.1 Geometrical configuration and boundary conditions

The 3D geometrical model of microchannel heat sink and its flow domain with teardrop dimples are shown in Fig. 1 .The width and height of the microchannel are 200 μm and 50 μm respectively. Dimples/protrusions are distributed in an aligned arrangement on the lateral side, the width of which is 200 μm. The teardrop dimples/protrusions with positive eccentricity are chosen as the flowing controlling structures, because these cases have the better thermal performance according to the previous studies. Thus teardrop dimple and protrusion structures with relative depth of δ/D_h =0.2 and positive eccentricity of e/D_h =0.3 are chosen to be the simulation model in the present study. The brief description for the dimple and protrusion structure is shown in Fig. 2.

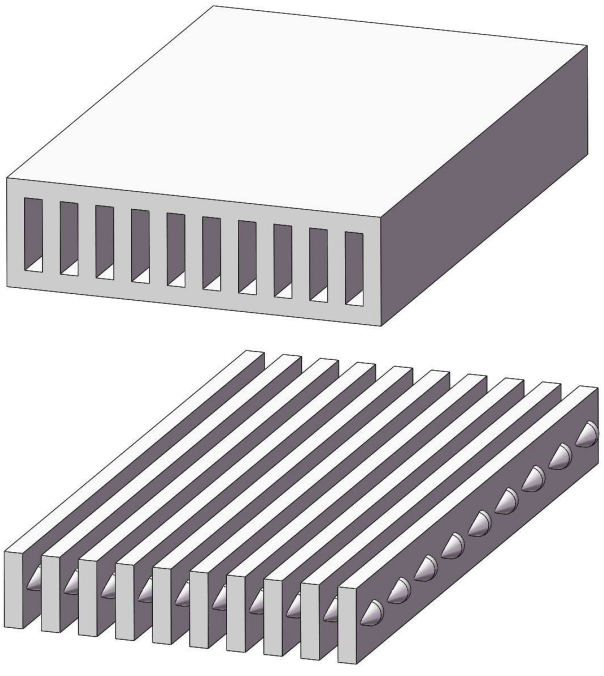

Figure 1: Three-dimensional model of heat sink and corresponding computational domain.

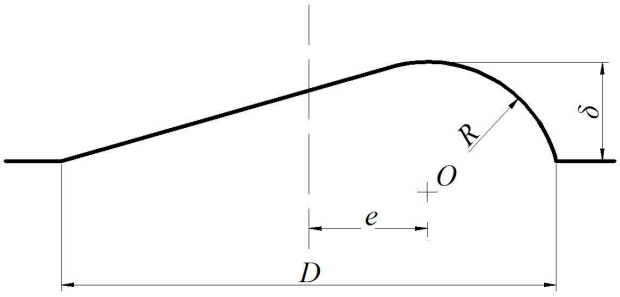

(a) dimple

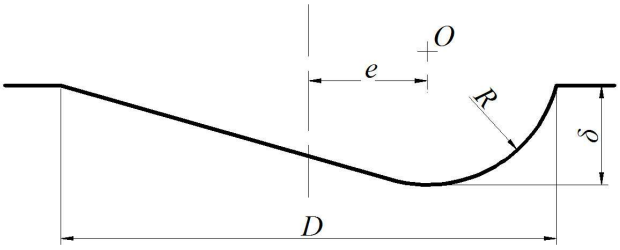

(b) protrusion

Figure 2: Geometry parameters of different structures.

The flow is assumed to be fully developed, steady and incompressible to simplify the governing equation in the simulation procedure. The computational domain is set to be a periodical module to save computing resources. The finite-volume method is adopted to solve the incompressible steady Navier-Stokes equations. The computations are regarded to be converged when the residual error of continuity, energy, velocity and the area-averaged wall temperature are less than 1×10^{-6}, 1×10^{-7}, 1×10^{-4} and 1×10^{-6} respectively. The specific geometry parameters of dimples and protrusions are shown in Fig. 2. Besides, the streamwise spacing is also 200 μm. The schematic diagram of boundary conditions of computational unit is shown in Fig. 3. The inlet and outlet is set as a periodic symmetrical boundary. The constant heat flux on the wall is equal to 5×10^5 W/m^{-2} and a No slip wall condition is applied. The flow velocity is increasing from 1.41 m/s to 8.69 m/s in this computation. The O-grids are applied for the teardrop structure region to improve the mesh quality. The refined mesh is applied around the flow boundary to improve the calculation accuracy. A part of the mesh distribution around the teardrop structures is shown in Fig. 4.

3.2 Data reduction

The hydraulic diameter is defined by

$$D_h = \frac{2WH}{W+H} \tag{5}$$

Table 2: Physical properties of Al_2O_3-Water nanofluids.

φ,%	C_p (J·kg^{-1}·K^{-1})	ρ(kg·m^{-3})	λ(W·m^{-1}·K^{-1})	k (Pa·s^n)	n
0.5	4161.93	1011.97	0.61	0.00187	0.88
1.5	4127.79	1041.69	0.63	0.00283	0.78
2.5	4093.65	1071.42	0.64	0.00426	0.68
3.5	4059.51	1101.15	0.66	0.00641	0.58
4.5	4025.37	1130.88	0.68	0.00876	0.50

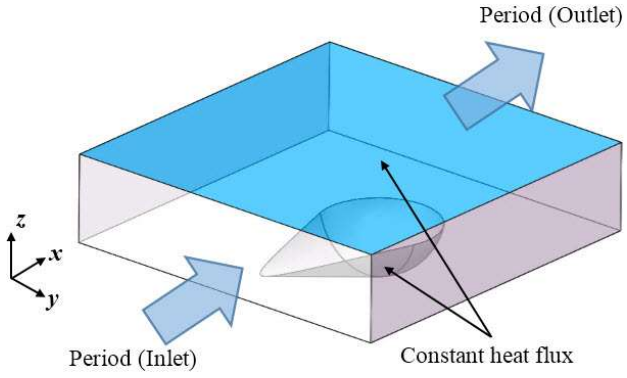

Figure 3: Boundary condition of the computation unit.

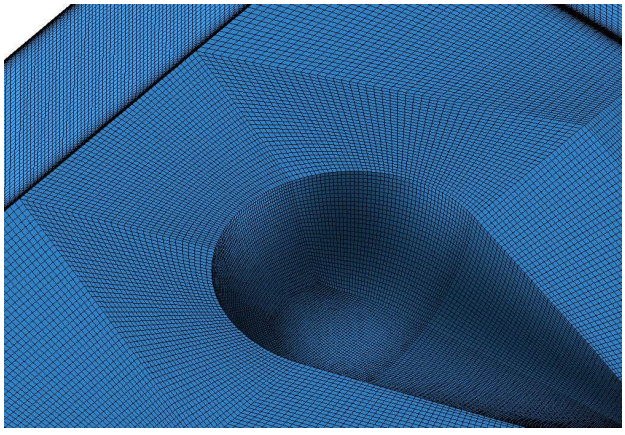

(a) trailing edge

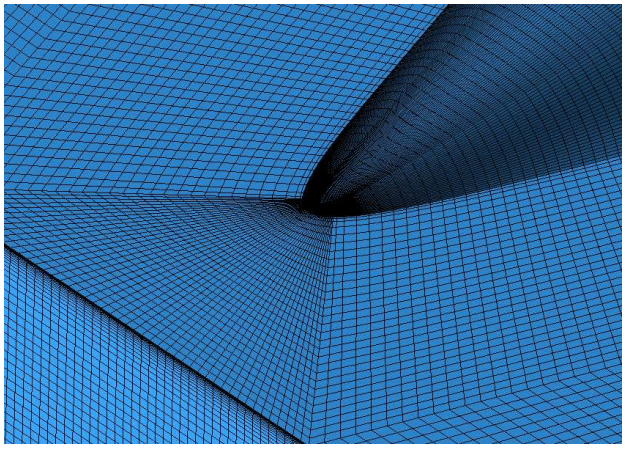

(b) leading edge

Figure 4: Mesh distribution of computation unit.

where W and H represents the width and height of cross section of microchannel respectively. The Reynolds number of non-Newtonian fluids is defined as [21]

$$Re = \frac{D_h^n U_{in}^{2-n} \rho}{k} \tag{6}$$

where ρ and U_{in} are the density and inlet average velocity respectively.

The average Nusselt number of the wall is determined by:

$$Nu = \frac{q}{\Delta T} \cdot \frac{D_h}{\lambda} \tag{7}$$

where λ represents the thermal conductivity. ΔT is the average temperature difference between fluid and wall, which is defined by the following equation [22]:

$$\Delta T = \frac{(T_{w,inlet} - T_{f,inlet}) - (T_{w,outlet} - T_{f,outlet})}{\ln\left[(T_{w,inlet} - T_{f,inlet})/(T_{w,outlet} - T_{f,outlet})\right]} \tag{8}$$

where the subscripts 'w' and 'f' represent wall and fluid respectively. According to the former literature, the Fanning friction factor, which is determined by eq. (9), can be used to describe the degree of pressure loss.

$$f = -\frac{(\Delta p/L) D_h}{2\rho U_{in}^2} \tag{9}$$

where Δp is the average difference between inlet pressure and outlet pressure. The thermal performance, which is proposed to evaluate the overall effect of heat transfer, is defined by:

$$TP = \left(\frac{Nu}{Nu_0}\right) \cdot \left(\frac{f}{f_0}\right)^{-1/3} \tag{10}$$

where the subscript '0' represents the corresponding parameters of water flowing in the smooth microchannel cases with the same boundary condition.

3.3 Governing equations

The simplified three-dimensional Navier-Stokes equations are solved to characterize the details of flow and heat transfer. The simulations is conducted by using the commercial software FLUENT. It could be obtained that the maximum Reynolds number of the cases studied is less than 450, by using the physical properties and equations above. According to the assumption above, the cases investigated are steady-state laminar flow, of which the governing equations can be simplified as follows [22].

$$\frac{\partial \rho}{\partial t} + \frac{\partial \rho u_i}{\partial x_i} = 0 \tag{11}$$

$$\frac{\partial \rho u_i}{\partial t} + \frac{\partial \rho u_i u_j}{\partial x_i} = \rho g_i + F_i - \frac{\partial P}{\partial x_i} + \frac{\partial}{\partial x_i}(2\mu S_{ij}) \tag{12}$$

$$\frac{\partial \rho E_0}{\partial t} + \frac{\partial \rho u_i E_0}{\partial x_i} = \rho u_i F_i - \frac{\partial q_i}{\partial x_i} + \frac{\partial}{\partial x_i}(u T_{ij}) \tag{13}$$

where t, x, u, g and P are time, coordinate, velocity, gravity acceleration and pressure, respectively. F, T, E_0 and S are body force, surface force, total internal energy and strain rate tensor. i, j =1,2,3.

3.4 Grid independence validation

The grid independence validation is conducted using the AW0.5 solution flowing at the boundary conditions of U_{in} =1.41 m·s^{-1}, T_{in} =300 K and q =5×10^5 W·m^{-2}. Four different sets of grids are applied and the detailed comparison between given sets is shown in Table 3.

The relative discrepancies of *Nu* and f decrease gradually with the increase of nodes. It is shown that the discrepancies are small enough in the case of mesh 3. So mesh 3 is selected in the present investigation.

3.5 Numerical method validation

In order to verify the numerical method, the data reported in the literature [17] is regarded as the reference. The flow and heat transfer in the corresponding smooth microchannel is simulated by the numerical procedure applied in the investigation. In the validation, a kind of shear- thinning fluid with n =1, k =10^{-3} Pa·s^n is chosen as the working substance. The rectangular microchannel scaled 200 μm×50 μm×150 μm is selected to be the computational domain. The boundary condition of q =5×10^5 W·m^{-2} and T_{in} =300 K is applied and the average inlet velocity varies from 1.41 m·s^{-1} to 8.69 m·s^{-1}.

Table 4 shows the comparison of the *Nu* and *fRe* between referenced and proposed model. The maximum deviation is 0.88% for *Nu* and 0.92% for *fRe* respectively, which shows the proposed model is feasible for the simulations in the present investigation.

4 Results and discussions

4.1 Flow characteristics

The limiting streamline distribution and temperature contours on the teardrop dimpled and protrusioned surface for AW0.5 nanofluids are presented in Fig. 5 and Fig. 6. For dimpled structures, the narrow leading edge makes streamline distorted at the front region. Under the effect of pressure gradient, a part of fluids deviates from the mainstream direction and impinges directly onto the trailing section of the teardrop dimple and then reverses. This part of fluids interacts with the mainflow at the core zones of teardrop structure, which leads to the relatively low pressure and a large backward vortex. It can be seen that there is apparent mass exchange and heat transfer. It should be noticed that when U_{in} =1.41 m·s^{-1}, the reverse point of limiting streamline is not at the rear edge of dimple, mainly because the effect of low pressure is bigger than that of mainflow inertia inside the dimple and the reverse point moves down. With the increase of the velocity, the radian of the flow separation line increase gradually. As shown in the case of U_{in} =8.69 m·s^{-1}, the area of the vortex zone is almost as big as the teardrop dimple and the radian of the separation line is large enough to distort the streamline around the rear section. The limiting streamline distribution basically keeps symmetrical in all cases. It is shown that the temperature of flow impinging zones and the trailing section is apparently lower than that of flow separation zones.

As seen from the figures, the working substance moving through the teardrop protrusion region shows symmetrical fusiform flow structure. At the leading edge, the flow moves along the teardrop protrusion surface and the velocity of nanofluids increases gradually because of the area decrease at cross section. As shown in Fig. 6, there is apparent vortex and flow separation at the trailing edge and the size of vortex zone becomes bigger as the velocity increases. As seen from the contours, the temperature at the back region of the protrusion structure is a little bit higher, which indicates that the flow separation weakens the heat transfer and mass exchange. As the velocity increases, the influence from backflow to mainflow grows bigger, which

Table 3: Grid independence validation.

Mesh	Nodes	*Nu*	Difference,%	*f*	Difference,%
1	792792	3.161	0.1684	1.622	0.282
2	1357884	3.178	0.1162	1.624	0.179
3	2404630	3.159	0.0962	1.627	0.0083
4	4571555	3.156		1.627	

Table 4: Numerical method validation.

U_{in} (m·s^{-1})	*Nu*		Deviation %	*fRe*		Deviation %
	Referenced	Proposed		Referenced	Proposed	
1.41	2.94	2.914	0.88	18.233	18.324	0.50
3.72	2.94	2.961	0.71	18.233	18.401	0.92
6.21	2.94	2.923	0.58	18.233	18.175	0.32
8.69	2.94	2.935	0.17	18.233	18.341	0.59

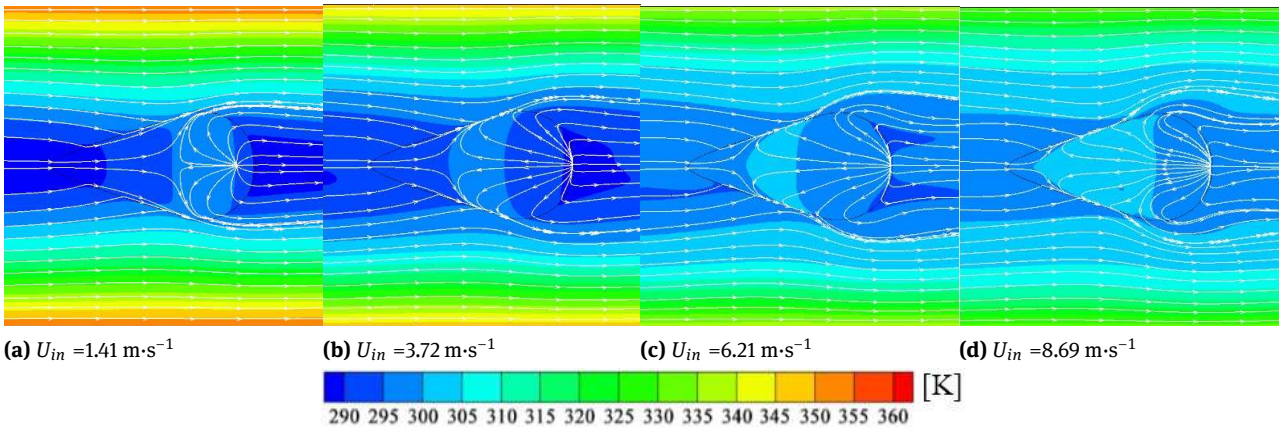

Figure 5: Limiting streamline and temperature contour on the teardrop dimple surface for AW0.5.

leads to the distortion of the limiting streamlines as shown in the case of U_{in} =8.69 m·s^{-1}.

The distribution of streamline and temperature counter on the streamwise middle section at U_{in} =1.41 m·s^{-1} with four non-Newtonian nanofluids, as displayed in Fig. 7 and Fig. 8, illustrates the flow characteristics from another point of view. It is clearly found that at the same inlet velocity, the size of vortex grows gradually with the increase of the solution volume fraction. When the non-Newtonian fluids flow through the teardrop dimple region, the special structure produces low pressure, which makes the flow moves down and forms vortex. It should be noticed that there appears secondary flow structure caused by the non-Newtonian shear thinning effects in the dimple region for the solution of φ =3.5%.

As shown in Fig. 8, the flow structure indicates that the vortex appears at the back region of the protrusion structure, because of the flow separation caused by the adverse pressure gradients. With the solution volume fraction increases, the size of the backflow vortex grows gradually bigger. As stated above, the existence of the rear vortex leads to the weakness of the mass exchange and heat transfer, so the temperature in this region is little higher than others. However, the temperature of the mainflow is apparently lower compared with the flow in dimpled channel at the same condition, mainly because the protrusion structure, diminishing the cross section area, makes the velocity increase and enhances the heat transfer of the mainflow. Meanwhile, with the increase of the volume fraction, the temperature of the mainflow is increasing gradually, which indicates the secondary flow effect of non-Newtonian fluids weakens the local heat transfer.

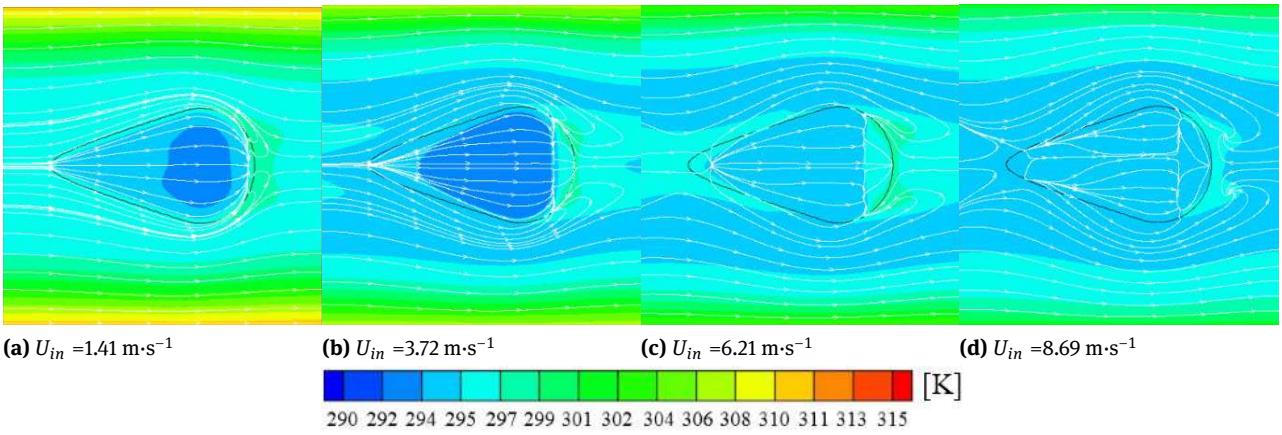

Figure 6: Limiting streamline and temperature contour on the teardrop protrusion surface for AW0.5.

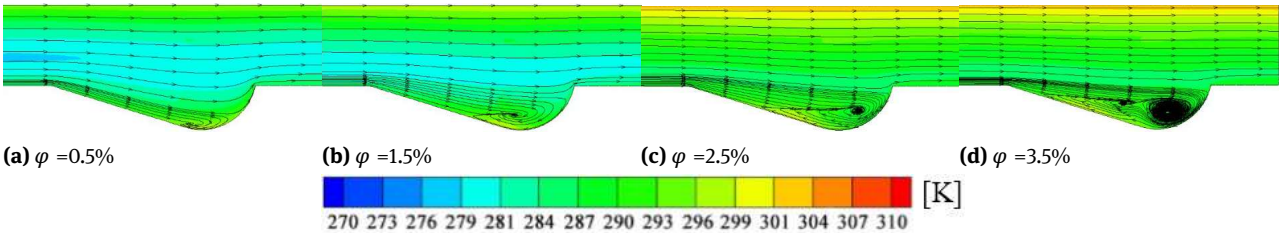

Figure 7: Distributions of streamlines and temperature on the streamwise middle sections at U_{in} =1.41 m·s^{-1} for dimpled microchannels.

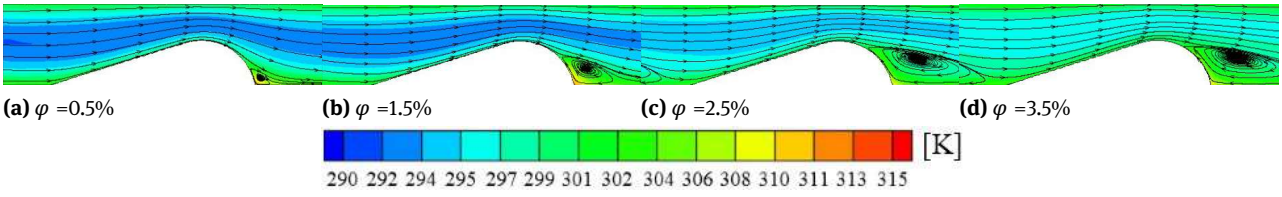

Figure 8: Distributions of streamlines and temperature on the streamwise middle sections at U_{in} =1.41 m·s^{-1} for protrusioned microchannels.

4.2 Heat transfer characteristics

The variations of relative Nusselt number Nu/Nu_0 based on the flow of water in smooth channel at same boundary conditions, with the inlet velocity for four solutions are shown in Fig. 7 and Fig. 8 respectively. The relative Nusselt number increases steadily with increasing velocity and the values for all the cases discussed in the present study are bigger than 1.0, which means teardrop dimple and protrusion structures effectively strengthen the heat transfer of Al_2O_3-water nanofluids compared with water flow. As stated before, a bigger volume fraction leads to a larger vortex in the teardrop dimple/protrusion region, which makes AW2.5 and AW3.5 have better heat transfer performance. Meanwhile, the increasing ratio of AW3.5 is larger than that of AW2.5 for the flow in dimpled microchannel. In the case of the protrusion, it can be seen that the higher volume fraction leads to better heat transfer performance.

4.3 Flow resistance characteristics

The variations of normal Fanning friction factor f/f_0 based on the flow of water in smooth passage are presented in Fig. 10. The f/f_0 for all the cases investigated in the present study increases with the growth of the inlet velocity. For the flow in dimpled/protrusioned microchannels, the f/f_0 of AW0.5 always shows the highest value and that of AW3.5 shows the lowest. As the volume fraction increases, the non-Newtonian shear thinning effect

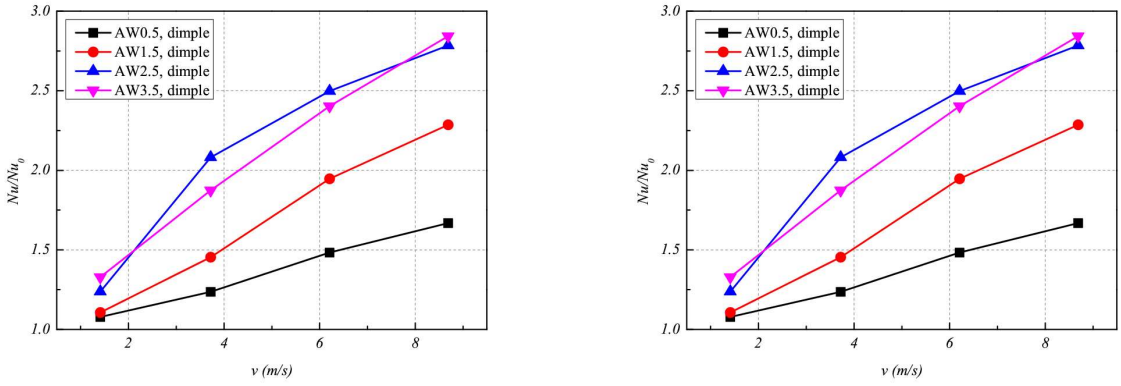

(a) dimpled microchannel **(b)** protrusioned microchannel

Figure 9: Normal Nusselt number Nu/Nu_0 variations with inlet velocity.

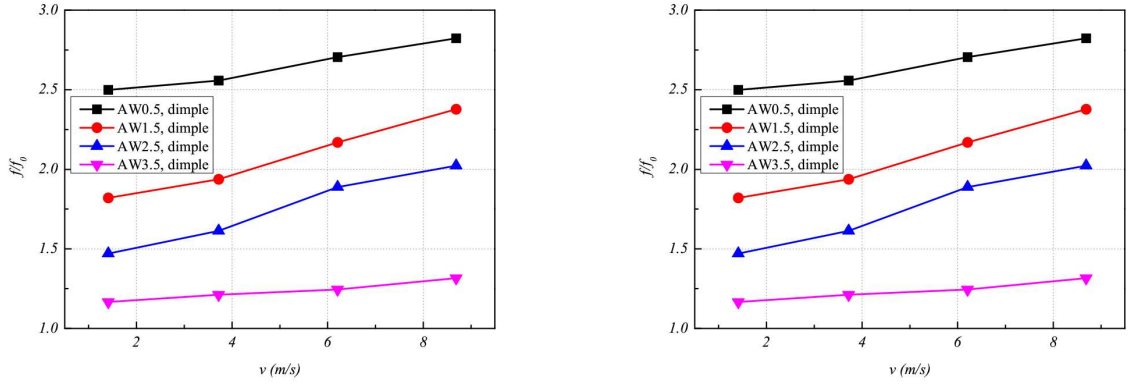

(a) dimpled microchannel **(b)** protrusioned microchannel

Figure 10: Normal Fanning friction factorf/f_0 variations with inlet velocity.

is strengthened gradually and the development of boundary layer is disturbed in advance, which makes AW3.5 show the best flow characteristics with low resistance loss among the cases discussed in the present study.

4.4 Thermal performance evaluation

It is known that *TP* is the parameter used to evaluate the heat transfer augmentation quantity [18, 19]. In order to obtain the overall thermal performance, the variation of *TP* with inlet velocity for all the cases studied is shown in Fig. 11. It is clearly found that *TP* for these four solutions in these two microchannels all increase gradually with the increase of the velocity. The values of most cases are bigger than 1.0, except the flow of AW0.5 and AW1.5 in dimpled microchannel at relatively low velocity. Comparing all the results, *TP* of AW0.5 is roughly the lowest and that of AW3.5 is the highest for the specific channel structure. The maximum value of *TP* has reached 2.59, which indicates AW solution has favorable overall thermal performance, compared with the flow of water in smooth microchannel. In the cases discussed in the present study, AW3.5 solution shows the best thermal performance in the dimpled and protrusioned microchannel. Meanwhile, the increasing ratio of the *TP* of dimpled cases is mostly higher than that of protrusioned cases.

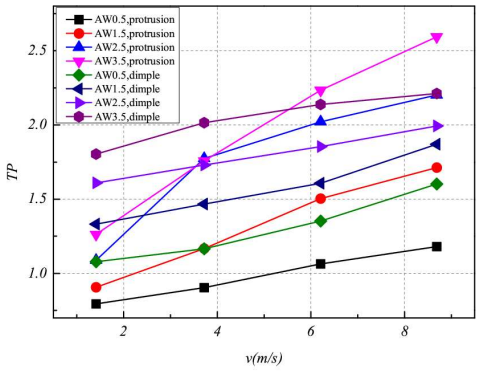

Figure 11: Thermal performance *TP* variations with inlet velocity.

4. The normalized Fanning friction factor f/f_0 increases with the inlet velocity, based on the flow of water in smooth microchannels. Solutions with higher volume fractions produce lower pressure loss at the same velocity due to the shear-thinning effects and the special flow structure.
5. *TP* increases gradually as the inlet velocity increases and AW3.5 solution shows the best thermal performance in most cases. The maximum of *TP* has reached 2.59. In order to obtain the best overall thermal performance, working substances with AW3.5 in the teardrop dimpled/protrusioned microchannel is preferred with the condition stated in the present study.

5 Conclusions

The flow structure and heat transfer behavior of Al_2O_3 aqueous solutions with four different volume fractions in the teardrop dimpled/protrusioned microchannel with positive eccentricity as e/D_h =0.3 and relative depth as δ/D_h =0.2 are investigated numerically. The following conclusions can be obtained.

1. The working substance flowing through the teardrop dimpled region is effected by pressure gradient and inertial force, which produces large vortex and backflow. As flow velocity and volume fraction increase, the size and intensity of vortex grows gradually. When the shear-thinning effect is large enough, there is secondary vortex in the dimple region. These characteristics enhance the exchange of mass and energy, which leads to the enhancement of overall thermal performance.
2. There is an apparent flow separation at the trailing edge of protrusion structures when the nanofluids flow through the channel. It is different from the dimpled cases in that the vortex caused by flow separation leads to the weakness of local heat transfer effect. However, the increase of mainstream velocity leads to the enhancement of the overall thermal performance.
3. Normalized Nusselt number Nu/Nu_0 is increasing as inlet velocity increases in the range of present study. Comparing all the values studied, the cases of AW2.5 and AW3.5 show the best thermal characteristics. Meanwhile all the values are larger than 1.0, which illustrated that Al_2O_3-water nanofluids have superior heat transfer performance than water flowing in smooth microchannel.

Nomenclature

C_p specific heat capacity, $J \cdot kg^{-1} \cdot K^{-1}$
D dimple print diameter, μm
D_h charateristic length, μm
H height of cross section, μm
W width of cross section, μm
L streamwise length, μm
λ thermal conductivity, $W \cdot m^{-1} \cdot K^{-1}$
k power-law flow consistency index, $Pa \cdot s^n$
n power-law flow behavior index
Nu average Nusselt number over surface
P pressure, Pa
q heat flux, $W \cdot m^{-2}$
T temperature, K
U_{in} fluid inlet velocity, $m \cdot s^{-1}$
X_{wall} wall shear stress
μ viscosity, Pa·s
ρ density of the fluid, $kg \cdot m^{-3}$
φ volume fraction of nanoparticles
τ shear stress, N
γ shear rate, s^{-1}

Subscripts
f base fluid
nf nanofluid
p nanoparticle

References

[1] Mohammed H. A., Bhaskaran G., Shuaib N. H., et al., Heat transfer and fluid flow characteristics in microchannels heat exchanger using nanofluids: a review, J. Renewable and Sustainable Energy Reviews., 2011, 15(3), 1502–1512.

[2] Sheremet M. A., Pop I., Conjugate natural convection in a square porous cavity filled by a nanofluid using Buongiorno's mathematical model, J. International Journal of Heat and Mass Transfer., 2014, 79, 137–145.
[3] Kefayati G. H. R., Heat transfer and entropy generation of natural convection on non-Newtonian nanofluids in a porous cavity, J. Powder Technology., 2016, 299, 127–149.
[4] Bourantas G. C., Skouras E. D., Loukopoulos V. C., et al., Heat transfer and natural convection of nanofluids in porous media, J. European Journal of Mechanics-B/Fluids., 2014, 43, 45–56.
[5] Sheremet M. A., Pop I., Bachok N., Effect of thermal dispersion on transient natural convection in a wavy-walled porous cavity filled with a nanofluid: Tiwari and Das' nanofluid model, J. International Journal of Heat and Mass Transfer., 2016, 92, 1053–1060.
[6] Rashidi M. M., Rastegari M. T., Asadi M., et al., A study of non-Newtonian flow and heat transfer over a non-isothermal wedge using the homotopy analysis method, J. Chemical Engineering Communications., 2012, 199(2), 231–256.
[7] Singh P. K., Harikrishna P. V., Sundararajan T., et al., Experimental and numerical investigation into the hydrodynamics of nanofluids in microchannels, J. Experimental Thermal and Fluid Science., 2012, 42, 174–186.
[8] Kalteh M., Abbassi A., Saffar-Avval M., et al., Experimental and numerical investigation of nanofluid forced convection inside a wide microchannel heat sink, J. Applied Thermal Engineering., 2012, 36, 260–268.
[9] Wen D., Ding Y., Experimental investigation into convective heat transfer of nanofluids at the entrance region under laminar flow conditions, J. International journal of heat and mass transfer., 2004, 47(24), 5181–5188.
[10] Santra A. K., Sen S., Chakraborty N., Study of heat transfer due to laminar flow of copper–water nanofluid through two isothermally heated parallel plates, J. International Journal of Thermal Sciences., 2009, 48(2), 391–400.
[11] Hatami M., Ganji D. D., Natural convection of sodium alginate (SA) non-Newtonian nanofluid flow between two vertical flat plates by analytical and numerical methods, J. Case Studies in Thermal Engineering., 2014, 2, 14–22.
[12] Li P., Zhang D., Xie Y., et al., Flow structure and heat transfer of non-Newtonian fluids in microchannel heat sinks with dimples and protrusions, J. Applied Thermal Engineering., 2016, 94, 50–58.
[13] Chyu M. K., Yu Y., Ding H., et al., Concavity enhanced heat transfer in an internal cooling passage, C. ASME 1997 International Gas Turbine and Aeroengine Congress and Exhibition. American Society of Mechanical Engineers, 1997, V003T09A080-V003T09A080.
[14] Chyu M. K., Yu Y., Ding H., Heat transfer enhancement in rectangular channels with concavities, J. Journal of Enhanced Heat Transfer., 1999, 6(6).
[15] Xie Y., Qu H., Zhang D., Numerical investigation of flow and heat transfer in rectangular channel with teardrop dimple/protrusion, J. International Journal of Heat and Mass Transfer., 2015, 84, 486–496.
[16] Lee P. S., Garimella S. V., Liu D., Investigation of heat transfer in rectangular microchannels, J. International Journal of Heat and Mass Transfer., 2005, 48(9), 1688–1704.
[17] Shah R. K., London A. L., Laminar flow forced convection in ducts: a source book for compact heat exchanger analytical data, M. Academic press, 2014.
[18] Xie G., Liu J., Zhang W., et al., Numerical prediction of flow structure and heat transfer in square channels with dimples combined with secondary half-size dimples/protrusions, J. Numerical Heat Transfer., Part A: Applications, 2014, 65(4), 327–356.
[19] Murata A., Mochizuki S., Centrifugal buoyancy effect on turbulent heat transfer in a rotating two-pass smooth square channel with sharp 180-deg turns, J. International journal of heat and mass transfer., 2004, 47(14), 3215–3231.
[20] Singh A. K., Harinadha G., Kishore N., et al., Mixed Convective Heat Transfer Phenomena of Circular Cylinders to Non-Newtonian Nanofluids Flowing Upward, J. Procedia Engineering., 2015, 127, 118–125.
[21] Nejat A., Mirzakhalili E., Aliakbari A., et al., Non-Newtonian power-law fluid flow and heat transfer computation across a pair of confined elliptical cylinders in the line array, J. Journal of Non-Newtonian Fluid Mechanics., 2012, 171, 67–82.
[22] Qu H., Shen Z., Xie Y., Numerical Investigation of Flow and Heat Transfer in a Dimpled Channel among Transitional Reynolds Numbers, J. Mathematical Problems in Engineering., 2013, 2013.